Proceedings of IDETC/CIE 2005
ASME 2005 International Design Engineering Technical Conferences and Computers and Information in Engineering Conference
September 24-28, 2005, Long Beach, California, USA

DETC2005-84580

MODELING AND SIMULATION OF AN ELASTIC SHIP-MOUNTED CRANE

Yousef Al-Sweiti *
Engineering Faculty
Institute for Mechatronics and System Dynamics
University Duisburg-Essen
Lotharstraße 1, 47057 Duisburg, Germany
Email: alsweiti@uni-duisburg.de

Dirk Söffker
Engineering Faculty
Institute for Mechatronics and System Dynamics
University Duisburg-Essen
Lotharstraße 1, 47057 Duisburg, Germany
Email: soeffker@uni-duisburg.de

ABSTRACT

This paper deals with development and simulation of the nonlinear model of an elastic ship-mounted crane equipped with the Maryland Rigging. The model contains three inputs to control the planar vibrations due to the planar base excitation; the luff angle is proposed to control the elastic vibration in the boom, and the length of the upper cable in conjunction with the position of its lower suspension point are proposed to control the pendulation of the payload. It is observed, through static and dynamic testing of the derived model, that moving the lower suspension point of the upper cable provides strong controllability of the horizontal displacement of the payload, while changing the length of the cable can be employed to compensate for the vertical displacement. Simulation results show that within a considerable range of pendulation displacements of the payload, the nonlinear model and the linearized one reflect nearly equivalent responses. Hence, with the property of strong controllability, the linear model can be used efficiently to design the control system, which will be discussed later in another paper.

INTRODUCTION

This work focuses on the mathematical modeling and simulation of an elastic ship-mounted crane with Maryland Rigging as shown in Fig. 1. Such a crane is usually used to transfer cargo from one ship to another in an open sea. During the transfer process, wave-induced motions of the crane can produce large oscillations of the cargo being hoisted, which endanger the operation of the crane and force the cargo transfer to be suspended.

This problem is discussed in the last few years in several publications. Yuan et al. [1] proposed the "Maryland's Rigging" and applied a brake system to the upper cable as it passes over the pulley, Kimiaghalam et al. [2] proposed a fuzzy controller to limit the pendulation of the payload by changing the length of the upper cable, Dadone and Van Landingham [3] proposed fuzzy logic for controlling the Coulomb friction in the pulley, Kimiaghalam et al. [4] proposed feedback and feedforward control law to change the luff angle and the length of the rope. Abdel-Rahman and Nayfeh [5] examined the in-plane and out-of-plane responses of the crane to an in-plane excitation and a control effort limited to dry friction and viscous damping applied at the pulley. In the mentioned publications, the authors based their modeling and design on the assumptions that the boom of the crane is rigid, and the actuators are strong enough to provide the calculated control inputs. In the real world, these assumptions may be difficult to realize because the rigid boom is usually massive, which means that it may be hard to execute fast motions of the boom as calculated and commanded by the controller.

To contribute in solving this problem, an elastic lighter weight boom is considered, and a small modification in the configuration of the crane is proposed by adding a limited degree of mobility to the lower suspension point of the upper cable on which the pulley rides.

The finite element method is used to model the elastic boom dynamics, which is coupled with the dynamics of the pulley and the payload. The model employs three independents inputs to stabilize the crane operation in the plane of the boom; the luff angle to control the elastic vibration, and the total length of the upper cable in addition to the position of its lower suspension point to control the pendulation of the payload. The model is limited to the in-plane oscillations because those are dangerous in practical applications. The disturbances acting on boom due to ship movements are represented by exciting

horizontal and vertical displacements $x_A(t)$ and $y_A(t)$ applied directly to the lower end of the elastic boom as shown in Fig. 1.

MODEL DEVELOPMENT

In deriving the mathematical model of the crane, the following assumptions are considered:

- The lower part of the boom (part *AB*) is elastic, while the upper part (part *BC*) is rigid.
- The elongation in the cables and the structural damping are neglected.
- The lower suspension point *B'* of the upper cable is movable along the rigid part of the boom.
- The pulley (m_1) is frictionless.
- The payload (m_2) is considered as a point mass and the air resistance is neglected.
- The luff angle $\beta(t)$ is actuated by the moment M_A applied directly to the lower end of the boom (*A*).

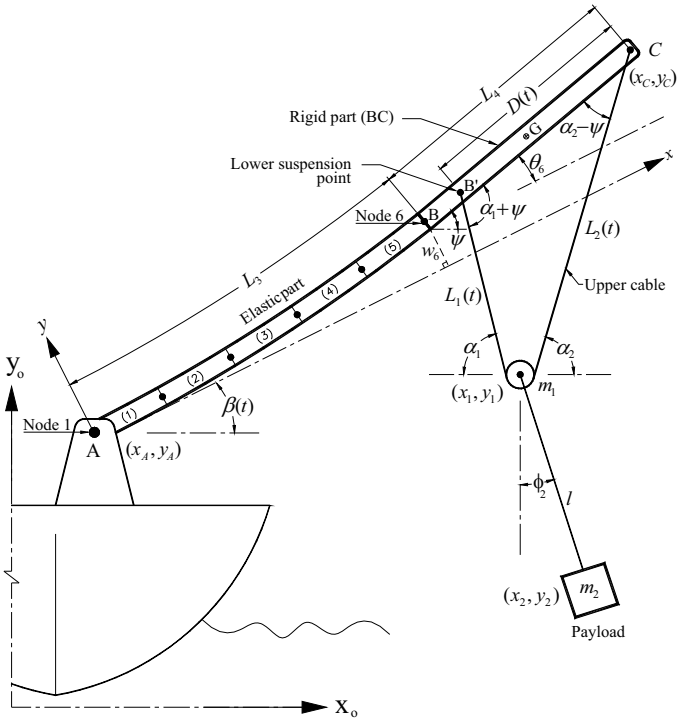

Figure 1. Elastic Maryland rigged boom crane

Kinematics of the upper cable

With reference to Fig. 1, assume that L_1 and L_2 are the distances between the pulley and the lower and upper suspension points (*B* and *C*) respectively. By applying the sine law, these distances can be expressed as

$$L_1 = D\,s(\alpha_2 - \psi)\csc(\alpha_1 + \alpha_2) \tag{1}$$

$$L_2 = D\,s(\alpha_1 + \psi)\csc(\alpha_1 + \alpha_2) \tag{2}$$

and the total length of the cable is given by

$$\begin{aligned} L(t) &= L_1 + L_2 \\ &= D\,c(\psi + \frac{\alpha_1 - \alpha_2}{2})\sec(\frac{\alpha_1 + \alpha_2}{2}) \end{aligned} \tag{3}$$

where *s* and *c* are the abbreviations for the trigonometric sine and cosine functions respectively, α_1 and α_2 are the angles of L_1 and L_2 with respect to the horizontal, D is the position of the movable suspension point *B'* along the portion *BC* with respect to the tip of the boom, and

$$\psi = \beta + \theta_6 \tag{4}$$

is the planar orientation of *BC* with respect to the horizontal, and θ_6 the elastic rotational displacement at node 6, which represents the end point of the elastic portion of the boom. Manipulating Eq. (3) and utilizing the trigonometric relations to isolate α_1 yields

$$\tan\frac{\alpha_1}{2} = \frac{L\,c\,\frac{\alpha_2}{2} - D\,c(\frac{\alpha_2}{2} - \psi)}{L\,s\,\frac{\alpha_2}{2} + D\,s(\frac{\alpha_2}{2} - \psi)}. \tag{5}$$

Therefore

$$\frac{\alpha_1}{2} = \text{Atan2}\left[\left(Lc\frac{\alpha_2}{2} - Dc(\frac{\alpha_2}{2} - \psi)\right), \left(Ls\frac{\alpha_2}{2} + Ds(\frac{\alpha_2}{2} - \psi)\right)\right], \tag{6}$$

where Atan2(y,x) is the arctangent function of two arguments; it computes the arctangent of the ratio y/x but utilizes the sign of each argument to determine which quadrant the resulting angle belongs to.

In order to eliminate α_1 from L_2, Eq. (2) is written as

$$L_2 = D\left(\frac{s\alpha_1\,c\psi + c\alpha_1\,s\psi}{s\alpha_1\,c\alpha_2 + c\alpha_1\,s\alpha_2}\right), \tag{7}$$

Using the trigonometric transformations, the above equation gives the compact expression of the length L_2 as

$$L_2 = \frac{1}{2}\left(\frac{L^2 - D^2}{L - D\,c(\alpha_2 - \psi)}\right). \tag{8}$$

Differentiating Eq. (8) with respect to time gives

$$\dot{L}_2 = \gamma_1\,\dot{L} + \gamma_2\,\dot{D} + \gamma_3\,(\dot{\alpha}_2 - \dot{\beta} - \dot{\theta}_6) \tag{9}$$

$$\ddot{L}_2 = \gamma_1\,\ddot{L} + \gamma_2\,\ddot{D} + \gamma_3\,(\ddot{\alpha}_2 - \ddot{\beta} - \ddot{\theta}_6) + f_2, \tag{10}$$

with

$$\gamma_1 = \frac{L^2 + D^2 - 2DL\,c(\alpha_2 - \psi)}{2[L - D\,c(\alpha_2 - \psi)]^2}$$

$$\gamma_2 = \frac{[L^2 + D^2]\,c(\alpha_2 - \psi) - 2DL}{2[L - D\,c(\alpha_2 - \psi)]^2}$$

$$\gamma_3 = \frac{[D^3 - DL^2]\, s(\alpha_2 - \psi)}{2[L - D\, c(\alpha_2 - \psi)]^2}$$

$$f_2 = \dot{\gamma}_1 \dot{L} + \dot{\gamma}_2 \dot{D} + \dot{\gamma}_3 (\dot{\alpha}_2 - \dot{\beta} - \dot{\theta}_6). \tag{11}$$

Kinematics of the pulley

The global position of the pulley can be described as

$$x_1 = x_C - L_2\, c\alpha_2 \tag{12}$$

$$y_1 = y_C - L_2\, s\alpha_2\,, \tag{13}$$

with

$$x_C = x_A + L_3\, c\beta - w_6\, s\beta + L_4\, c\psi \tag{14}$$

$$y_C = y_A + L_3\, s\beta + w_6\, c\beta + L_4\, s\psi\,, \tag{15}$$

where x_C and y_C are the coordinates of the tip of the boom with respect to the inertial reference frame, and w_6 is the transverse displacement of point B with respect to the x-axis of the boom. Differentiating Eqs. (12) and (13) twice with respect to time gives the acceleration components of the pulley as

$$\ddot{x}_1 = \ddot{x}_C - \ddot{L}_2\, c\alpha_2 + 2\dot{L}_2\, \dot{\alpha}_2\, s\alpha_2 + L_2(\ddot{\alpha}_2\, s\alpha_2 + \dot{\alpha}_2^2\, c\alpha_2) \tag{16}$$

$$\ddot{y}_1 = \ddot{y}_C - \ddot{L}_2\, s\alpha_2 - 2\dot{L}_2\, \dot{\alpha}_2\, c\alpha_2 - L_2(\ddot{\alpha}_2\, c\alpha_2 - \dot{\alpha}_2^2\, s\alpha_2)\,. \tag{17}$$

Kinematics of the payload

The global position of the payload is expressed as

$$x_2 = x_1 + l\, s\phi_2 \tag{18}$$

$$y_2 = y_1 - l\, c\phi_2, \tag{19}$$

which can be differentiated twice with respect to time to give the absolute velocity and acceleration of the payload as

$$\ddot{x}_2 = \ddot{x}_1 + l\, c\phi_2\, \ddot{\phi}_2 - l\, s\phi_2\, \dot{\phi}_2^2 \tag{20}$$

$$\ddot{y}_2 = \ddot{y}_1 + l\, s\phi_2\, \ddot{\phi}_2 + l\, c\phi_2\, \dot{\phi}_2^2\,. \tag{21}$$

Kinetics of the payload

Consider the free body diagram of the payload as shown in Fig. 2. Applying Newton's second law in x-and y-directions leads to

$$-T_3\, s\phi_2 = m_2\, \ddot{x}_2 \tag{22}$$

$$T_3\, c\phi_2 - m_2 g = m_2\, \ddot{y}_2\,, \tag{23}$$

where T_3 is the tension in the payload cable.
Using Eq. (23) to eliminate T_3 from Eq. (22) and inserting Eqs. (20) and (21) in the resulted equation gives the differential equation of m_2 in implicit form as

$$m_2 \ddot{x}_1\, c\phi_2 + m_2 l \ddot{\phi}_2 + m_2 (g + \ddot{y}_1)\, s\phi_2 = 0, \tag{24}$$

which in view of Eqs. (16) and (17) gives the full nonlinear differential equation of the payload in explicit form as

$$\begin{aligned}
&- m_2 s(\beta - \phi_2)\, \ddot{w}_6 + m_2[\gamma_3\, c(\alpha_2 - \phi_2) - L_4 s(\psi - \phi_2)]\ddot{\theta}_6 \\
&+ m_2[\gamma_3 c(\alpha_2 - \phi_2) - L_3 s(\beta - \phi_2) - w_6 c(\beta - \phi_2) - L_4 s(\psi - \phi_2)]\ddot{\beta} \\
&- m_2 \gamma_1\, c(\alpha_2 - \phi_2)\, \ddot{L} - m_2 \gamma_2\, c(\alpha_2 - \phi_2)\, \ddot{D} \\
&+ m_2[L_2\, s(\alpha_2 - \phi_2) - \gamma_3\, c(\alpha_2 - \phi_2)]\ddot{\alpha}_2 \\
&+ m_2 l \ddot{\phi}_2 + m_2\, c\phi_2\, \ddot{x}_A + m_2\, s\phi_2\, \ddot{y}_A + m_2 g\, s\phi_2 - m_2 f_2 c(\alpha_2 - \phi_2) \\
&- 2m_2 \dot{w}_6 \dot{\beta}\, c(\beta - \phi_2) - m_2 \dot{\beta}^2 [L_3\, c(\beta - \phi_2) - w_6\, s(\beta - \phi_2)] \\
&- m_2 L_4 \dot{\psi}^2\, c(\psi - \phi_2) + m_2 L_2 \dot{\alpha}_2^2\, c(\alpha_2 - \phi_2) \\
&+ 2m_2\, s(\alpha_2 - \phi_2)\, \dot{\alpha}_2[\gamma_1\, \dot{L} + \gamma_2\, \dot{D} + \gamma_3\, \dot{\alpha}_2 - \gamma_3\, \dot{\psi}] = 0\,.
\end{aligned} \tag{25}$$

Kinetics of the pulley

Consider the free body diagram of the pulley in Fig. 2. Since the pulley is assumed as frictionless, the tension in L_1 is equal to the tension in L_2. Hence, applying Newton's second law in x_1 and y_1 directions gives

$$T\,(c\alpha_2 - c\alpha_1) + T_3\, s\phi_2 = m_1 \ddot{x}_1 \tag{26}$$

$$T\,(s\alpha_1 + s\alpha_2) - m_1 g - T_3\, c\phi_2 = m_1 \ddot{y}_1\,. \tag{27}$$

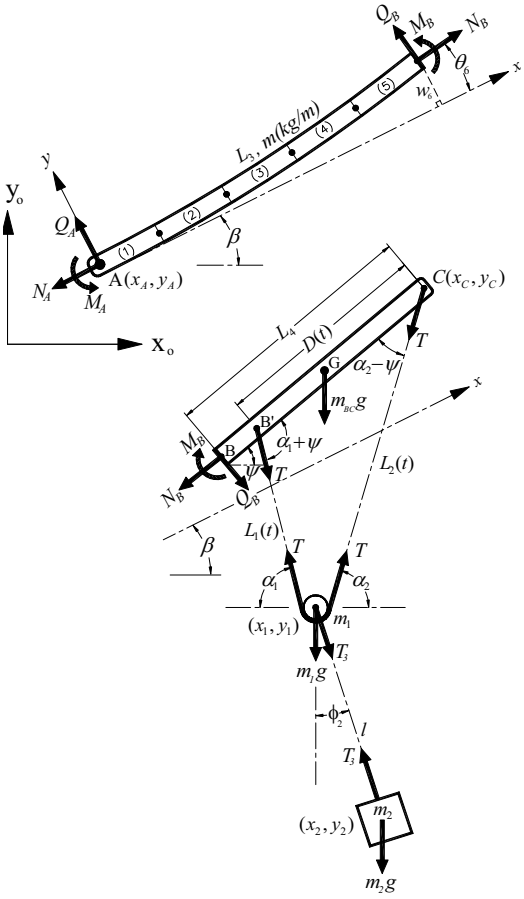

Figure 2: Free body diagram of the elastic and rigid parts

Substituting Eq. (23) into Eq. (27) and utilizing Eq. (21) yields the magnitude of the tension in the upper cable as

$$T = \frac{(m_1 + m_2)(g + \ddot{y}_1) + m_2(l\ddot{\phi}_2 s\phi_2 + l\dot{\phi}_2^2 c\phi_2)}{s\alpha_1 + s\alpha_2}. \tag{28}$$

Substituting Eqs. (28), (22) into Eq. (26) and using Eq. (20) gives the full nonlinear equation of motion of the pulley in implicit form

$$\left(\frac{c\alpha_2 - c\alpha_1}{s\alpha_1 + s\alpha_2}\right)\left[(m_1 + m_2)(g + \ddot{y}_1) + m_2(l\ddot{\phi}_2\, s\phi_2 + l\dot{\phi}_2^2\, c\phi_2)\right] - (m_1 + m_2)\ddot{x}_1 - m_2 l\ddot{\phi}_2\, c\phi_2 + m_2 l\dot{\phi}_2^2\, s\phi_2 = 0. \tag{29}$$

Using the trigonometric transformations, it can be shown that

$$\left(\frac{c\alpha_2 - c\alpha_1}{s\alpha_1 + s\alpha_2}\right) = \tan\left(\frac{\alpha_1 - \alpha_2}{2}\right), \tag{30}$$

which can be inserted into Eq. (29) to give

$$\begin{aligned} &Mg\, s\left(\frac{\alpha_1 - \alpha_2}{2}\right) - m_2 l\ddot{\theta}_2\, c\left(\phi_2 + \frac{\alpha_1 - \alpha_2}{2}\right) \\ &+ m_2 l\dot{\phi}_2^2\, s\left(\phi_2 + \frac{\alpha_1 - \alpha_2}{2}\right) \\ &+ M\left[s\left(\frac{\alpha_1 - \alpha_2}{2}\right)\ddot{y}_1 - c\left(\frac{\alpha_1 - \alpha_2}{2}\right)\ddot{x}_1\right] = 0. \end{aligned} \tag{31}$$

where $M = (m_1 + m_2)$. Using Eqs. (9) and (10) to eliminate $\dot{L}_2$ and $\ddot{L}_2$ from Eqs. (16) and (17), and substituting the result in Eq. (31) gives the full nonlinear differential equation of m_1 as

$$\begin{aligned} &M\, s\left(\beta + \frac{\alpha_1 - \alpha_2}{2}\right)\ddot{w}_6 + M[L_4\, s\left(\psi + \frac{\alpha_1 - \alpha_2}{2}\right) \\ &- \gamma_3 c\left(\frac{\alpha_1 + \alpha_2}{2}\right)]\ddot{\theta}_6 + M[L_3 s\left(\beta + \frac{\alpha_1 - \alpha_2}{2}\right) + w_6 c\left(\beta + \frac{\alpha_1 - \alpha_2}{2}\right) \\ &+ L_4\, s\left(\psi + \frac{\alpha_1 - \alpha_2}{2}\right) - \gamma_3 c\left(\frac{\alpha_1 + \alpha_2}{2}\right)]\ddot{\beta} + M\gamma_1\, c\left(\frac{\alpha_1 + \alpha_2}{2}\right)\ddot{L} \\ &+ M\gamma_2\, c\left(\frac{\alpha_1 + \alpha_2}{2}\right)\ddot{D} + M[\gamma_3 c\left(\frac{\alpha_1 + \alpha_2}{2}\right) - L_2 s\left(\frac{\alpha_1 + \alpha_2}{2}\right)]\ddot{\alpha}_2 \\ &- m_2 l\, c\left(\phi_2 + \frac{\alpha_1 - \alpha_2}{2}\right)\ddot{\phi}_2 - Mc\left(\frac{\alpha_1 - \alpha_2}{2}\right)\ddot{x}_A + Ms\left(\frac{\alpha_1 - \alpha_2}{2}\right)\ddot{y}_A \\ &+ Mg\, s\left(\frac{\alpha_1 - \alpha_2}{2}\right) + m_2 l\dot{\phi}_2^2\, s\left(\phi_2 + \frac{\alpha_1 - \alpha_2}{2}\right) + Mf_2\, c\left(\frac{\alpha_1 + \alpha_2}{2}\right) \\ &+ 2M\dot{w}_6\dot{\beta}\, c\left(\beta + \frac{\alpha_1 - \alpha_2}{2}\right) + ML_4\dot{\psi}^2\, c\left(\psi + \frac{\alpha_1 - \alpha_2}{2}\right) \\ &+ M\dot{\beta}^2[L_3 c\left(\beta + \frac{\alpha_1 - \alpha_2}{2}\right) - w_6 s\left(\beta + \frac{\alpha_1 - \alpha_2}{2}\right)] \\ &- 2Ms\left(\frac{\alpha_1 + \alpha_2}{2}\right)\dot{\alpha}_2[\gamma_1\dot{L} + \gamma_2\dot{D} + \gamma_3\dot{\alpha}_2 - \gamma_3\dot{\psi}] \\ &- ML_2\dot{\alpha}_2^2 c\left(\frac{\alpha_1 + \alpha_2}{2}\right) = 0. \end{aligned} \tag{32}$$

One important aspect to be mentioned here is that choosing the angular coordinates α_1 and α_2 results in an explicit and relatively short differential equation for m_1 (Eq. 32), which can be too long if the cartesian coordinates are used instead.

Dynamics of the rigid part (*BC*)

As shown in Fig. 1, the position of the center of gravity of member *BC* with respect to the inertial reference frame O-$x_0y_0z_0$ can be represented as

$$\mathbf{G} = G_{x0}\,\hat{\mathbf{x}}_0 + G_{y0}\,\hat{\mathbf{y}}_0, \tag{33}$$

where $\hat{\mathbf{x}}_0$ and $\hat{\mathbf{y}}_0$ are unit vectors in the directions x_0 and y_0 respectively, with

$$G_{x0} = x_A + L_3\, c\beta - w_6\, s\beta + \frac{L_4}{2} c\psi \tag{34}$$

$$G_{y0} = y_A + L_3\, s\beta + w_6\, c\beta + \frac{L_4}{2} s\psi. \tag{35}$$

The component of the acceleration of point G in the lateral direction of the boom can be expressed as

$$\begin{aligned} \ddot{G}_y &= \ddot{G}_{y0}\, c\beta - \ddot{G}_{x0}\, s\beta \\ &= -\ddot{x}_A\, s\beta + \ddot{y}_A\, c\beta + \ddot{w}_6 + \frac{L_4}{2} c\theta_6\, \ddot{\theta}_6 \\ &\quad + (L_3 + \frac{L_4}{2} c\theta_6)\ddot{\beta} - w_6\dot{\beta}^2 - \frac{L_4}{2}\dot{\psi}^2\, s\theta_6. \end{aligned} \tag{36}$$

Applying Newton's second law to member *BC* (Fig. 2) in the lateral direction gives

$$-Q_B - T\left[s(\alpha_1 + \beta) + s(\alpha_2 - \beta)\right] - m_{BC} g\, c\beta = m_{BC}\,\ddot{G}_y, \tag{37}$$

where m_{BC} denotes the mass of member *BC*, and Q_B is the shear force at point *B*. Substituting Eqs. (28) and (36) in Eq. (37) yields

$$\begin{aligned} Q_B = &-m_{BC}[g\, c\beta - \ddot{x}_A\, s\beta + \ddot{y}_A\, c\beta + \ddot{w}_6 + 0.5L_4\, c\theta_6\, \ddot{\theta}_6 \\ &+ (L_3 + 0.5L_4 c\theta_6)\ddot{\beta}] + m_{BC} w_6\dot{\beta}^2 + 0.5 m_{BC} L_4\dot{\psi}^2 s\theta_6 \\ &+ H[M(g + \ddot{y}_1) + m_2 l(\ddot{\phi}_2\, s\phi_2 + \dot{\phi}_2^2\, c\phi_2)] \end{aligned} \tag{38}$$

with

$$H = s\beta\tan\left(\frac{\alpha_1 - \alpha_2}{2}\right) - c\beta. \tag{39}$$

By eliminating $\ddot{y}_1$ from Eq. (38) the explicit expression of the shear force at the boundary between the elastic the elastic and rigid parts can be expressed as

$$
\begin{aligned}
Q_B &= -[m_{BC} - MH\,c\beta]\ddot{w}_6 \\
&-[0.5m_{BC}L_4c\theta_6 - MH(L_4c\psi + \gamma_3 s\alpha_2)]\ddot{\theta}_6 \\
&-[m_{BC}(L_3 + 0.5L_4c\theta_6) - MH(L_3c\beta - w_6 s\beta + L_4c\psi + \gamma_3 s\alpha_2)]\ddot{\beta} \\
&- MH\gamma_1 s\alpha_2\ddot{L} - MH\gamma_2 s\alpha_2\ddot{D} - MH[\gamma_3 s\alpha_2 + L_2 c\alpha_2]\ddot{\alpha}_2 \\
&+ m_2 lH\, s\phi_2\ddot{\phi}_2 + m_{BC}\, s\beta\,\ddot{x}_A + [MH - m_{BC}\,c\beta]\ddot{y}_A \\
&-[m_{BC}\,c\beta - MH]g + m_{BC}[w_6\dot{\beta}^2 + 0.5L_4\dot{\psi}^2\, s\theta_6] \\
&- MH[s\alpha_2\, f_2 + 2\dot{w}_6\dot{\beta}\, s\beta + L_4\dot{\psi}^2 s\psi \\
&+ 2c\alpha_2\,\dot{\alpha}_2(\gamma_1\dot{L} + \gamma_2\dot{D} + \gamma_3\dot{\alpha}_2 - \gamma_3\dot{\psi}) - \dot{\alpha}_2^2 L_2\, s\alpha_2 \\
&+ \dot{\beta}^2(L_3\, s\beta + w_6\, c\beta)] + m_2 lH\dot{\phi}_2^2\, c\phi_2 .
\end{aligned} \tag{40}
$$

Similarly, the moment equation about point *B* can be written in the form

$$
\sum \mathbf{M}_B = I_{BC}\,\ddot{\psi}\,\hat{\mathbf{z}}_0 + \mathbf{r}_{BG} \times m_{BC}\,(\ddot{G}_{x0}\,\hat{\mathbf{x}}_0 + \ddot{G}_{y_0}\,\hat{\mathbf{y}}_0) \tag{41}
$$

with

$$
\mathbf{r}_{BG} = 0.5L_4[c\psi\,\hat{\mathbf{x}}_0 + s\psi\,\hat{\mathbf{y}}_0]. \tag{42}
$$

Therefore, the final expression of the bending moment at point *B* can be expressed as

$$
\begin{aligned}
M_B &= -[MP\,c\beta + 0.5m_{BC}L_4c\theta_6]\ddot{w}_6 \\
&-[I_{BC} + 0.25m_{BC}L_4^2 + MP(L_4\,c\psi + \gamma_3\,s\alpha_2)]\ddot{\theta}_6 \\
&-[I_{BC} + 0.5m_{BC}L_4(L_3\,c\theta_6 + w_6\,s\theta_6 + 0.5L_4) \\
&+ MP(L_3\,c\beta - w_6\,s\beta + L_4\,c\psi + \gamma_3\,s\alpha_2)]\ddot{\beta} \\
&+ MP\gamma_1 s\alpha_2\,\ddot{L} + MP\gamma_2 s\alpha_2\ddot{D} + MP[\gamma_3 s\alpha_2 + L_2 c\alpha_2]\ddot{\alpha}_2 \\
&- m_2 lP\, s\phi_2\,\ddot{\phi}_2 + 0.5\,m_{BC}L_4 s\psi\,\ddot{x}_A - [MP + 0.5\,m_{BC}L_4 c\psi]\ddot{y}_A \\
&-[MP + 0.5\,m_{BC}L_4 c\psi]g \\
&- 0.5\,m_{BC}L_4[2\dot{w}_6\dot{\beta}\, s\theta_6 - \dot{\beta}^2(w_6 c\theta_6 - L_3 s\theta_6)] \\
&+ MP[s\alpha_2\, f_2 + 2\dot{w}_6\dot{\beta}\, s\beta + L_4\dot{\psi}^2 s\psi + \dot{\beta}^2(L_3\, s\beta + w_6\, c\beta) \\
&+ 2c\alpha_2\,\dot{\alpha}_2(\gamma_1\dot{L} + \gamma_2\dot{D} + \gamma_3\dot{\alpha}_2 - \gamma_3\dot{\psi}) - \dot{\alpha}_2^2 L_2\, s\alpha_2] \\
&- m_2 lP\,\dot{\phi}_2^2\, c\phi_2,
\end{aligned} \tag{43}
$$

with

$$
P = \frac{(L_4 - D)\,s(\alpha_1 + \psi) + L_4\,s(\alpha_2 - \psi)}{s\alpha_1 + s\alpha_2}. \tag{44}
$$

In view of the free body diagram of the elastic part (Fig. 2), the calculated Q_B and M_B can be considered as the exciting loads which couple the dynamics of the elastic and rigid parts together.

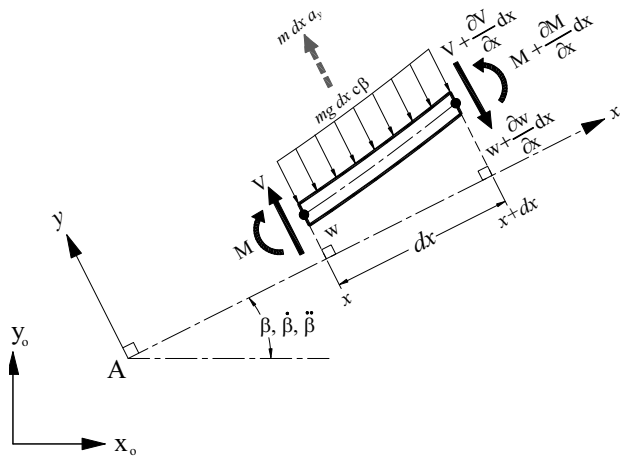

Figure 3: Geometry of a single boom element, all axial force components are neglected.

Dynamics of the elastic part (*AB*)

For deriving the finite element model of the elastic part, the effects of rotary inertia, transverse shear deformation, and the axial force are neglected. Accordingly, with reference to the single element shown in Fig. 3, the equation of motion in *y*-direction has the form

$$
\frac{\partial V}{\partial x} + ma_y = -mg\,c\beta\,, \tag{45}
$$

where m represents the mass per unit length of the boom and a_y is the absolute lateral acceleration of the element located at x, such that

$$
a_y = \frac{\partial^2 w}{\partial t^2} + x\ddot{\beta} + \ddot{y}_A c\beta - \ddot{x}_A s\beta\,. \tag{46}
$$

Substituting Eq. (46) into Eq. (45) and utilizing the relation

$$
V = \frac{\partial}{\partial x}\left(EI\,\frac{\partial^2 w}{\partial x^2}\right) \tag{47}
$$

gives

$$
\frac{\partial^2}{\partial x^2}\left(EI\,\frac{\partial^2 w}{\partial x^2}\right) + m\frac{\partial^2 w}{\partial t^2} = p(x,t), \tag{48}
$$

where

$$
p(x,t) = -m\ddot{\beta}\,x - m[(g + \ddot{y}_A)c\beta - \ddot{x}_A\,s\beta] \tag{49}
$$

represents the distributed lateral load acting on the part *AB*.

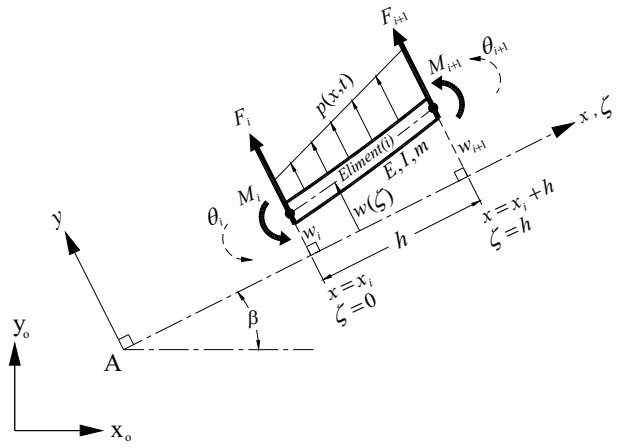

Figure 4: Single finite element

Figure 4 shows the free body diagram of a single finite element of length h, the element force vector (acting on the nodes i and $i+1$) can be expressed as

$$\mathbf{f}_e = [F_i \;\; M_i \;\; F_{i+1} \;\; M_{i+1}]^T = \int_0^h p(x,t)\,\mathbf{N}_e\, d\zeta, \tag{50}$$

where $\mathbf{N}_e$ is the 4×1 cubic interpolation functions vector which relates the transverse displacement $w(\zeta)$ to the node variables vector $\boldsymbol{\upsilon}_e = [w_i \;\; \theta_i \;\; w_{i+1} \;\; \theta_{i+1}]^T$ [6]. The element mass and stiffness matrices are also defined as

$$\mathbf{M}_e = \int_0^h m\,\mathbf{N}_e\,\mathbf{N}_e^T d\zeta \tag{51}$$

$$\mathbf{K}_e = \int_0^h EI\,\mathbf{N}_e''\,\mathbf{N}_e''^T d\zeta\,, \tag{52}$$

where $\mathbf{N}_e''$ denotes the second derivative of $\mathbf{N}_e$ with respect to the local coordinate ζ.

Since $p(x,y)$ varies linearly with the position of the element (x), each element has a different force vector whose magnitude depends on the location of the element along the boom. Therefore, to calculate the integration in the right hand side of Eq. (50), equation (49) can be rewritten as

$$p(x,t) = -m\ddot{\beta}\,(x_i + \zeta) - f_0, \tag{53a}$$

with

$$f_0 = m[(g + \ddot{y}_A)c\beta - \ddot{x}_A s\beta], \tag{53b}$$

where $0 \le \zeta \le h$ is the local longitudinal axis of the element, and x_i locates the element under consideration with respect to point A as shown in Fig. 4. Then, inserting Eq. (53a) into Eq. (50) and carrying out the integration yields

$$\mathbf{f}_e = -\frac{h}{20}\begin{bmatrix} 10f_0 + m\ddot{\beta}\,(10x_i + 3h) \\ \frac{5}{3}hf_0 + \frac{mh}{3}\ddot{\beta}\,(5x_i + 2h) \\ 10f_0 + m\ddot{\beta}\,(10x_i + 7h) \\ -\frac{5}{3}hf_0 - \frac{mh}{3}\ddot{\beta}\,(5x_i + 3h) \end{bmatrix}. \tag{54}$$

By dividing the boom into five elements (i = 1,…,5), the mass matrix, the stiffness matrix, and the nodal force vector can be easily constructed by the assembling process [6] to give the equations of motion that governs the elastic vibrations as

$$\mathbf{M}\,\ddot{\boldsymbol{\upsilon}} + \mathbf{K}\,\boldsymbol{\upsilon} = \mathbf{F}, \tag{55}$$

where $\mathbf{M}$ and $\mathbf{K}$ are the 12×12 constant symmetric mass and stiffness matrices respectively, $\mathbf{F}$ is the 12×1 nodal force vector and

$$\boldsymbol{\upsilon} = [w_1 \;\; \theta_1 \;\; w_2 \;\; \theta_2 \;\; \cdots \;\; w_6 \;\; \theta_6]^T \tag{56}$$

is the 12×1 nodal displacement vector with w_i and θ_i representing the nodal translational rotational displacements respectively at node i with respect to the x-axis of the boom.

It is obvious that the total load vector ($\mathbf{F}$) is equal to the nodal force vector $\mathbf{f}$ resulting from the assembling process due to $p(x,y)$ plus the force vector $\mathbf{r}$ due to the external loads at the boundaries (A and B) of the boom (Fig. 2), i.e.

$$\mathbf{F} = \mathbf{f} + \mathbf{r}, \tag{57}$$

with

$$\mathbf{f} = -\frac{h}{20}\begin{bmatrix} 10f_0 + 3mh\ddot{\beta} \\ \frac{5}{3}hf_0 + \frac{2}{3}mh^2\ddot{\beta} \\ 20f_0 + 20mh\ddot{\beta} \\ \frac{4}{3}mh^2\ddot{\beta} \\ 20f_0 + 40mh\ddot{\beta} \\ \frac{4}{3}mh^2\ddot{\beta} \\ 20f_0 + 60mh\ddot{\beta} \\ \frac{4}{3}mh^2\ddot{\beta} \\ 20f_0 + 80mh\ddot{\beta} \\ \frac{4}{3}mh^2\ddot{\beta} \\ 10f_0 + 47mh\ddot{\beta} \\ -\frac{5}{3}hf_0 - \frac{23}{3}mh^2\ddot{\beta} \end{bmatrix}, \tag{58}$$

and

$$\mathbf{r} = [Q_A \;\; M_A \;\; 0 \;\; 0 \;\; 0 \;\; 0 \;\; 0 \;\; 0 \;\; 0 \;\; 0 \;\; Q_B \;\; M_B]^T. \tag{59}$$

Because the boom is clamped at $x = 0$, the translational and rotational displacements must be zero, $w_1 = 0$ and $\theta_1 = 0$. Therefore, Eq. (55) can be partitioned to take the form

$$\begin{bmatrix} \mathbf{M}_{11} & \mathbf{M}_{12} \\ \mathbf{M}_{21} & \mathbf{M}_{22} \end{bmatrix} \begin{bmatrix} \ddot{\boldsymbol{\upsilon}}_1 \\ \ddot{\boldsymbol{\upsilon}}_2 \end{bmatrix} + \begin{bmatrix} \mathbf{K}_{11} & \mathbf{K}_{12} \\ \mathbf{K}_{21} & \mathbf{K}_{22} \end{bmatrix} \begin{bmatrix} \boldsymbol{\upsilon}_1 \\ \boldsymbol{\upsilon}_2 \end{bmatrix} = \begin{bmatrix} \mathbf{F}_1 \\ \mathbf{F}_2 \end{bmatrix}, \tag{60}$$

where

$$\boldsymbol{\upsilon}_1 = [w_1 \quad \theta_1]^T = [0 \quad 0]^T, \tag{61}$$

$$\boldsymbol{\upsilon}_2 = [w_2 \quad \theta_2 \quad \cdots \quad w_6 \quad \theta_6]^T. \tag{62}$$

In view of Eq. (60), the equations of motion of the boom can be expressed as

$$\mathbf{M}_{22}\ddot{\boldsymbol{\upsilon}}_2 + \mathbf{K}_{22}\boldsymbol{\upsilon}_2 = \mathbf{F}_2, \tag{63}$$

and the reaction force Q_A and the luff moment M_A at point A can be obtained from

$$\mathbf{M}_{12}\ddot{\boldsymbol{\upsilon}}_2 + \mathbf{K}_{12}\boldsymbol{\upsilon}_2 = \mathbf{F}_1 \tag{64}$$

Notice that, the force vector in Eq. (63) is coupled with the nonlinear differential equations of m_1 and m_2 through the boundary reactions Q_B and M_B, which are expressed previously in their final nonlinear form in Eqs. (40) and (43). These two equations can be used to eliminate Q_B and M_B from Eq. (63), which in conjunction with Eqs. (32) and (25) represent the nonlinear equations of motion of the complete crane. These equations contain the variables $\beta(t)$, $L(t)$, and $D(t)$ as inputs to control the vibrations in the crane. Notice also that in view of Eqs. (12,13, 18 and 19) and with the knowledge of $w_6, \theta_6, \alpha_2, \phi_2$ and the three inputs; the position of m_1 and m_2 with respect to the base of the boom (A) can be easily computed.

It may be more realistic to introduce the luff moment $M_A(t)$ instead of the luff angle $\beta(t)$ as an input to control the elastic vibrations in the boom. Therefore, the equation that relates them to each other can be directly extracted from Eq. (64) as

$$\frac{mh}{420}\left(13h\ddot{w}_2 - 3h^2\ddot{\theta}_2\right) + \frac{EI}{h^3}\left(-6hw_2 + 2h^2\theta_2\right) = -\frac{h}{60}\left(5hf_0 + 2mh^2\ddot{\beta}\right) + M_A. \tag{65}$$

This implies that $\beta(t)$ is now a generalized coordinate added to the other generalized coordinates of the system, which increases the order of the overall model by 2, and the full nonlinear mathematical model of the complete crane is the coupled Eqs. (65), (63), (32) and (25) with $M_A(t)$, $L(t)$, and $D(t)$ as control inputs and $\ddot{x}_A$ and $\ddot{y}_A$ as unwanted disturbance inputs.

Derivation of the equilibrium point

At the equilibrium point, it is clear that

$$\begin{aligned} \alpha_{10} &= \alpha_{20} \\ \phi_{20} &= 0, \end{aligned} \tag{66}$$

and the elastic translational and rotational displacements vector $(\boldsymbol{\upsilon}_0)$ can be computed from Eq. (55) by setting $\ddot{\boldsymbol{\upsilon}}$ and the time dependent terms in $\mathbf{F}$ equal to zero, i.e.

$$\boldsymbol{\upsilon}_0 = \mathbf{K}^{-1}\mathbf{F}_0. \tag{67}$$

By inserting Eq. (66) into Eq. (5) the magnitude of α_{20} can be expressed as

$$\alpha_{20} = \cos^{-1}\left(\frac{D_0}{L_0}c\psi_0\right), \tag{68}$$

where

$$\psi_0 = \beta_0 + \theta_{60}. \tag{69}$$

Similarly, the magnitude of M_{A0} can be calculated from Eq. (65) as

$$M_{A0} = \frac{EI}{h^3}\left(-6hw_{20} + 2h^2\theta_{20}\right) + \frac{5}{60}mgh^2c\beta_0. \tag{70}$$

Expanding the model about the equilibrium point

To study the complex nonlinear model, Taylor series is utilized to expand the nonlinear terms about the equilibrium point, which is characterized by Eqs. (66-70). Then, by keeping only linear and quadratic terms, the equations of motion of the crane can be written in the form

$$\mathbf{M}_0\ddot{\mathbf{q}} + \mathbf{K}_0\mathbf{q} = \mathbf{B}_1\mathbf{u}_c + \mathbf{B}_2\ddot{\mathbf{u}}_c + \mathbf{B}_d\ddot{\mathbf{u}}_d + \mathbf{n}, \tag{71}$$

where

$$\mathbf{q} = [\Delta w_2 \quad \Delta\theta_2 \quad \cdots \quad \Delta w_6 \quad \Delta\theta_6 \quad \Delta\beta \quad \Delta\alpha_2 \quad \Delta\phi_2]^T \tag{72}$$

is the 13×1 generalized displacement vector, and

$$\mathbf{u}_c = [\Delta M_A \quad \Delta L \quad \Delta D]^T \tag{73}$$

is the control input vector, and

$$\ddot{\mathbf{u}}_d = [\ddot{x}_A \quad \ddot{y}_A]^T \tag{74}$$

is the disturbance vector, $\mathbf{M}_0$ and $\mathbf{K}_0$ are 13×13 total mass and stiffness matrices respectively, $\mathbf{B}_1$ and $\mathbf{B}_2$ are 13×3 input matrices, $\mathbf{B}_d$ is the 13×2 disturbance matrix, and all nonlinear terms are collected in the 13×1 vector $\mathbf{n}$. The structure of $\mathbf{M}_0$, $\mathbf{K}_0$, $\mathbf{B}_1$, $\mathbf{B}_2$ and $\mathbf{B}_d$ is not explicitly described for the sake of conciseness.

The idea behind writing the equations of motion in the form given in Eq. (71) is to isolate the nonlinear terms in order to find analytically and by simulation which of them are important and which can be neglected; this is useful because it may be very difficult to design the control system for the current full nonlinear MIMO model due to its high complexity.

ANALYSIS AND SIMULATION RESULTS

Studying the influence of the variables L and D on the equilibrium position of the payload

With the computed generalized displacements at the equilibrium configuration, the equilibrium position of the payload with respect to the base of the crane can be calculated from Eqs. (18) and (19) such that

$$\begin{aligned} x_{20/A} &= (x_{20} - x_A) \\ &= L_3\, c\beta_0 - w_{60}\, s\beta_0 + L_4\, c\psi_0 - L_{20}\, c\alpha_{20} \end{aligned} \tag{75}$$

$$\begin{aligned} y_{20/A} &= (y_{20} - y_A) \\ &= L_3\, s\beta_0 + w_{60}\, c\beta_0 + L_4\, s\psi_0 - L_{20}\, s\alpha_{20} - l, \end{aligned} \tag{76}$$

where L_{20} can be computed from Eq. (8) as

$$L_{20} = \frac{1}{2}\left(\frac{L_0^2 - D_0^2}{L_0 - D_0\, c(\alpha_{20} - \psi_0)} \right). \tag{77}$$

To investigate the influence of the input variables in displacing the equilibrium position of the payload; the following parameters of a small model constructed for the task of experimentation are choozen:

$$\begin{aligned} &L_4 = 0.5\text{m},\ L_3 = 2L_4,\ h = L_3/5,\ l = L_4,\ L_0 = 4L_4, \\ &D_0 = 0.5L_4, g = 9.81\text{m/s}^2, m_2 = 5\text{kg},\ m_1 = 0.01m_2, \\ &m = 1.2\text{kg/m}, m_{BC} = 1.2\text{kg},\ I = 1.88\times10^{-9}\,\text{m}^4, \\ &I_{BC} = m_{BC}L_4^2/12,\ E = 207\text{GPa}. \end{aligned} \tag{78}$$

Figures 5 and 6 illustrate the influence of the variables L and D on displacing the equilibrium position of the payload for different values of β, it can be recognized from Figure 5 that for all possible values of β, changing L can efficiently displace y_{20} with a negligible effect on x_{20}. In addition, it can be noted from Figure 6 that for β < 1.0 rad., which is the normal operating configuration of the crane, the input D can change x_{20} considerably with a little effect on y_{20}. Therefore, it can be shown that the variable D can be used efficiently to control the horizontal coordinate x_2, whereas, the variable L can be employed to control the vertical coordinate y_2.

As a quick check to ascertain the capability of D to control the horizontal oscillation of the payload, the linearized open loop model ($\mathbf{n} = \mathbf{0}$) with β = π/4 and the given parameters in Eq. (78) are considered. By closing the loop using delayed feedback [7,8] of the horizontal displacement of the payload (Δx_2) and assigning roughly the value of the controller gain and the applied time delay such that $|\Delta D_{\max}| < 0.2$, it can be noted, as shown in Fig. 7, that the oscillation amplitude of the payload can be significantly reduced.

On the other hand, it can be easily confirmed that the crane is completely state controllable by rewriting Eq. (71) in the state canonical form and observing that the corresponding input matrix has no rows with zeros and/or linear dependent values for all values of β under consideration.

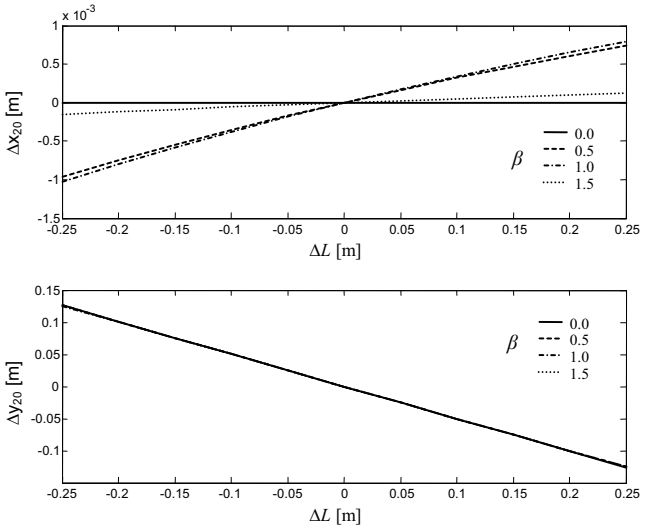

Figure 5. Effect of L on the equilibrium position of the payload for different β.

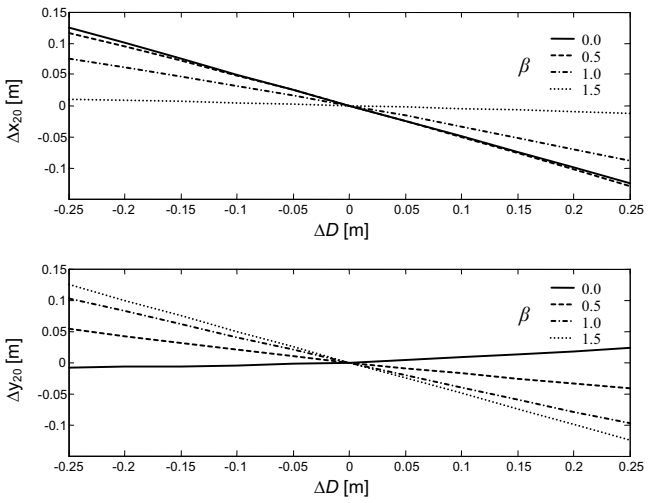

Figure 6. Effect of D on the equilibrium position of the payload for different β

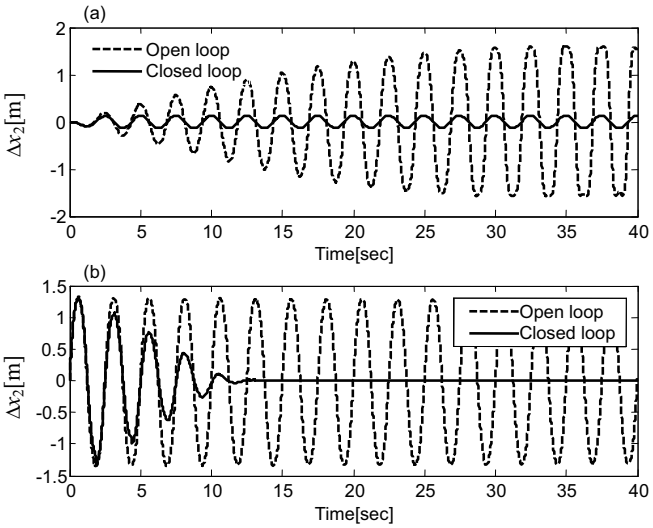

Figure 7. Influence of moving the lower suspension point in suppressing payload oscillation. (a) Due to a horizontal base excitation at the fundamental frequency of the crane, (b) due to a horizontal impulse force applied directly to m_2 .

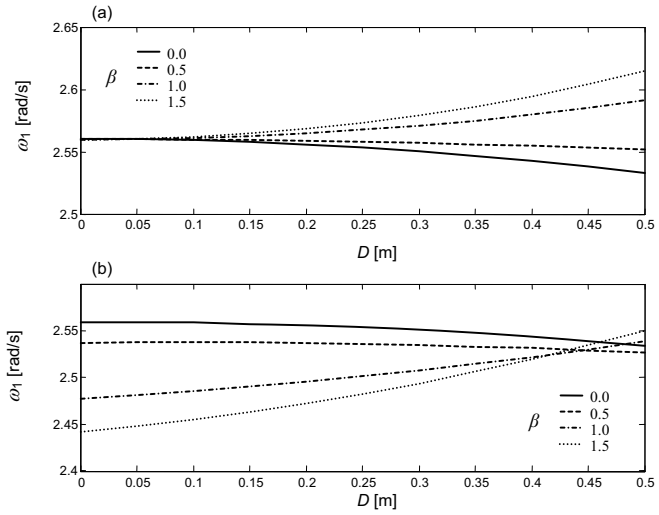

Figure 8. Effect of D and β on the fundamental Frequency of the crane

Effect of D and β on the fundamental frequency of the crane

Figure 8 illustrates the variation of the fundamental frequency with respect to changing D for different values of β. In Fig. 8(a), the boom is considered to be relatively rigid (EI is large). Therefore, it can be noted that the fundamental frequency undergoes a little decrement as the operating luff angle decreases; this is reasonable because of the geometrical behavior of the rigging, which produces lower restoring moment due to the lower ratio of the vertical displacement to the horizontal displacement of the pulley m_1 as β gets smaller. In Fig. 8(b), an elastic boom is considered, and it can be noted that the natural frequency is smaller for higher values of the luff angle because the horizontal component of the transverse deflection experienced by the boom, which is proportional to $\sin(\beta)$, has more contribution in affecting the side to side motion of the vibrating rigid components.

Effect of the nonlinear terms on the simulation results

To examine the effect of the nonlinear terms on the response of the crane in the operating range, the model is simulated for different values of β, L and D such that, in the first step, the full nonlinear model is simulated for several initial conditions and base excitations. In the next step, the nonlinear terms in $\mathbf{n}$ are eliminated and simulation is conducted again to find their influence in the overall response. Simulation results show that within a considerable operating amplitudes of the generalized displacements, the response of the nonlinear model is close to the linear one obtained by eliminating all nonlinear terms, i.e. by setting $\mathbf{n} = \mathbf{0}$. To mention a sample of these results, Figs. 9 and 10 illustrate the responses of the linearized and nonlinear model for $\beta = \pi/4$ and an initial velocity of $\dot{\phi}_2(0) = 5$ rad/s. It can be noted that the response of the linear model coincides with that of the nonlinear one with only a small difference, observed in the elastic displacements (as shown in w_6 and θ_6); this small difference can be ignored in the control system design process due to the complexity that may be introduced by considering such small nonlinear effects.

In Figs. 11 and 12 the linear and nonlinear responses due to horizontal base excitation at 95% of the fundamental frequency of the crane are shown, it is noted that the obtained results highlight those obtained previously in the free vibration case. Therefore, it is obvious that with the controllability of the crane, the linearized model can be used to find a suitable control law. On the other hand, the full nonlinear model can be used in addition to the linearized one to simulate the designed closed loop control system. This will be discussed in detail in another paper.

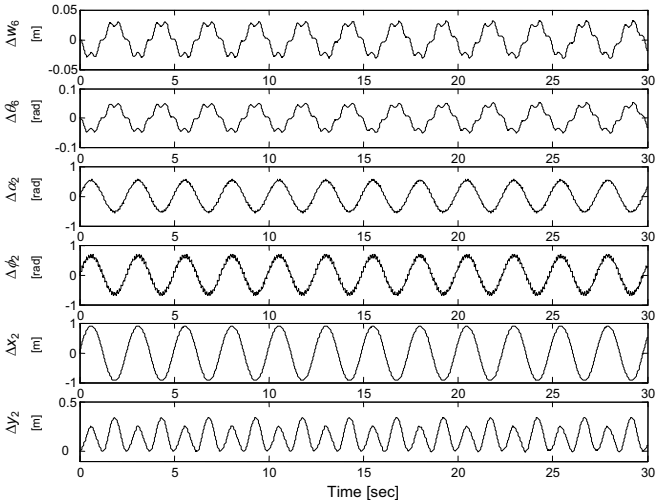

Figure 9. Linear response of the payload and the tip of the elastic boom, $\dot{\phi}_2(0) = 5\,\text{rad/s}$, β = π/4

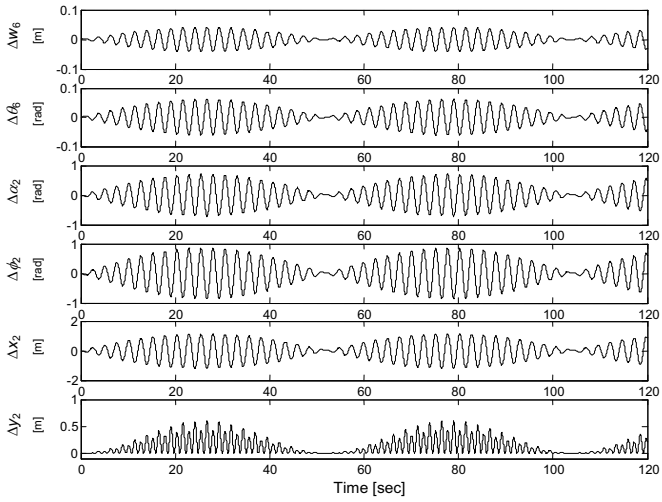

Figure 11. Linear response of the payload and the tip of the elastic boom, $\ddot{x}_A = 0.4\sin(0.95\,\omega_1 t)$, β = π/4

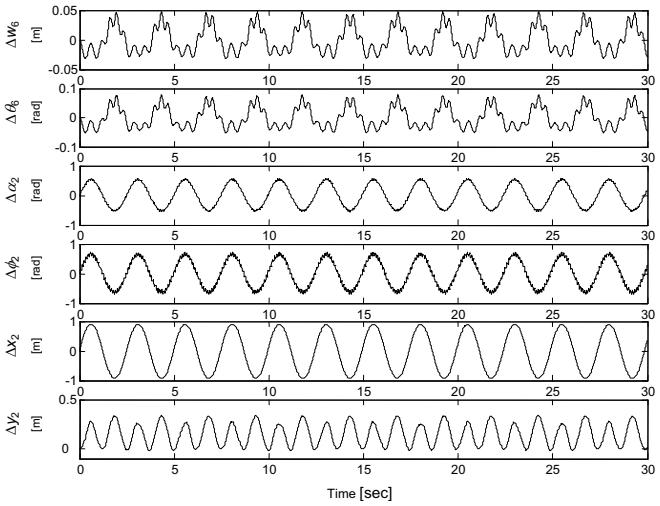

Figure 10. Nonlinear response of the payload and the tip of the elastic boom, $\dot{\phi}_2(0) = 5\,\text{rad/s}$, β = π/4

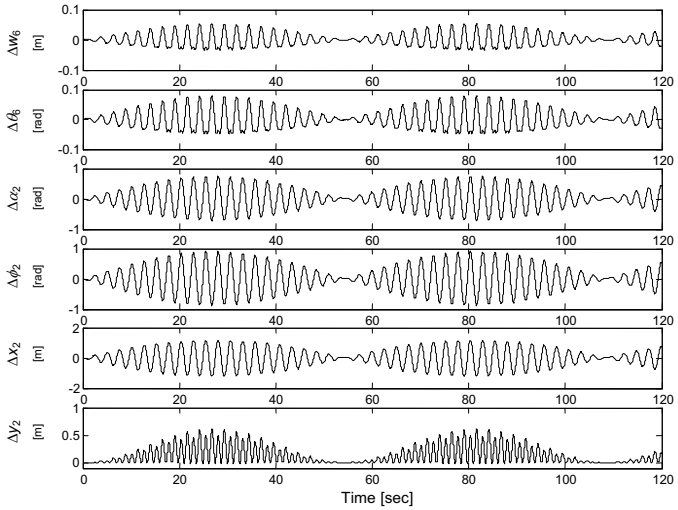

Figure 12. Nonlinear response of the payload and the tip of the elastic boom, $\ddot{x}_A = 0.4\sin(0.95\,\omega_1 t)$, β = π/4

CONCLUSIONS

The nonlinear equations of motion of the elastic crane are derived in their final explicit form, the nonlinear model is investigated by simulations for different values of crane parameters and the results were compared with those obtained from the linearized model about the corresponding equilibrium configuration. The results show that, within a considerable operating range of the generalized displacements, the linearized model can be used efficiently for the task of designing the control system of the crane.

ACKNOWLEDGMENTS

This work is supported by the German Academic Exchange Service (DAAD).

REFERENCES

[1] Yuan, G. H., Hunt, B. R., Grebogi, C., Ott, E., Yorke, J. A., and Kostelich, E. J., 1997, "Design and control of shipboard cranes," *DETC 97 Proceedings of the ASME Design Engineering Technical Conference*, Sacramento, CA, DETC97/VIB-4095.

[2] Kimiaghalam, B., Homaifar, A., and Bikdash, M., 1999, "Pendulation suppression of a shipboard crane using fuzzy controller," *Proceedings of the American Control Conference*, San Diego, CA, Vol. 1, pp. 586-590.

[3] Dadone, P. and Van Landingham, H. F., 1999, "The use of Fuzzy logic for controlling Coulomb friction in crane swing alleviation," *Intelligent Engineering Systems through Artificial Neural Networks* **9**, 751-756.

[4] Kimiaghalam, B., Homaifar, A., and Bikdash, M., 2000, "Feedback and feedforward control law for a ship crane with Maryland rigging system," *Proceedings of the American Control Conference*, Chicago, IL, Vol. 2, pp. 1047-1051.

[5] Abdel-Rahman, E. and Nayfeh, A., 2001, "Feasibility of two-dimensional control for ship-mounted cranes," *DETC 2001 Proceedings of the ASME Design Engineering Technical Conferences*, Pittsburgh, Pennsylvania, DETC 2001/VIB-21454.

[6] Meirovitch, L. 1986. *Elements of Vibration Analysis,* 2nd ed. McGraw-Hill Book Company, New York, Chap. 8, pp. 300-346.

[7] Masoud Z., Nayfeh, A., and Mook, D., 2004, "Cargo pendulation reduction of ship-mounted cranes," *Nonlinear dynamics* **35**, 299-311.

[8] Henry, R., Masoud Z., Nayfeh, A., and Mook, D., 2001, "Cargo pendulation reduction on ship-mounted cranes via boom-luff angle actuation," *Journal of vibration and control* **7**, 1253-1264.